

# Residual Stress in Metal Parts Produced by Powder-Bed Additive Manufacturing Processes

Xiaoqing Wang and Kevin Chou

Mechanical Engineering Department  
The University of Alabama  
Tuscaloosa, AL 35487

REVIEWED

## **Abstract:**

In this study, residual stresses from the electron beam additive manufacturing (EBAM) and selective laser melting (SLM) processes, due to repeated thermal cycles, were investigated. Residual stresses play a crucial role in part performance, and thus, it is critical to evaluate the process-induced residual stresses in AM parts. Ti-6Al-4V and Inconel 718 parts produced by EBAM and SLM, respectively, were studied in residual stresses using the methodology established by Carlsson et al., a mechanical instrumented indentation technique, which is based on the experimental correlation between the indentation characteristic and the residual stress. The results show that the Ti-6Al-4V EBAM parts have a compressive residual stress in both Z-plane and X-plane, while the Inconel 718 SLM parts show a tensile stress and a compressive stress in the Z-plane and X-plane, respectively. Besides, the Ti-6Al-4V parts have lower absolute value of residual stress than the Inconel 718 parts. Moreover, the Vickers hardness values of the parts built using SLM and EBAM are comparable to the literature data.

**Keywords:** Ti-6Al-4V, residual stress, Vickers indentation, microindentation, Electron Beam Additive manufacturing

## **Introduction:**

Additive manufacturing (AM) is currently one of the rapidly developing advanced manufacturing techniques in the world [1, 2]. As one of the family of AM technology, Electron beam additive manufacturing (EBAM), is one of a few AM technologies capable of making full-density metallic parts and has drastically extended AM applications for direct digital manufacturing of structural components [3]. In industries, Ti-6Al-4V is the most common titanium alloy being used due to its outstanding mechanical properties, such as high strength, high strength-to-weight ratio, good formability and heat treatability. The EBAM technology on Ti-6Al-4V has wide application in the industry, especially for aerospace components and medical implants. Besides, Selective laser melting (SLM), has been recognized as a promising AM technology, due to its flexibility in feedstock and shapes [4]. In SLM, a computer controlled scanning laser beam is applied as the energy source to melt the pre-spread powder particles selectively in a layer-by-layer manner [5, 6]. The geometrically complex components with high dimensional precision and good surface integrity can be obtained precisely by the SLM process without post-processing, which the conventional methods cannot keep pace with [7]. However, the repeated rapid heating and cooling processes will also result in the residual thermal stresses in the parts, which has a remarkable influence on the finish machining and the geometric resolution of the parts [8].

Residual stresses can be introduced into mechanical components during various thermal or thermo-mechanical processes such as heat treatment, forming, and welding [9-12]. Accurate evaluation of residual stresses is important because they play a crucial role in performance, integrity, and lifetime of the components. In other words, the residual stresses can strongly affect the mechanical performance (such as the static and fatigue strengths, fracture toughness, corrosion/wear resistance) and thus the reliability and lifetime of components and devices in a negative or positive way. Accordingly, various techniques for measuring residual stresses have been developed, such as X-ray and neutron diffractions, ultrasonic velocity, hole drilling, and layer removal techniques [13]. The sharp indentation or hardness testing is a well-known experimental method used for determination of the constitutive properties of conventional materials such as metals and alloys. Many studies have been undertaken to develop new ways to measure residual stress using instrumented indentation, because this non-destructive/mechanical technique may overcome the limitations of conventional methods including both the destructive/mechanical and nondestructive/ physical methods [14, 15].

Among all these methods, the instrumented indentation technique (IIT), has attracted intensive interest due to its simplicity, convenience and applicability at various scales. Tusi et al. [16] established a bilinear relation between hardness and residual stress. Numerous studies have also indicated that various indentation characteristic parameters, such as indentation depth (h), loading curvature (C), contact stiffness (S), and indentation work (W) present nonlinear relationship with residual stresses [17-20]. Based on experimental correlation between the indentation characteristic parameters and residual stress, several models for calculating the residual stresses based on the indentation characteristic parameters have been proposed, among which the models proposed by Suresh and Giannakopoulos [17], Carlsson and Larsson [18, 19], Lee and Kwon [21] and Wang et al. [22] are most representative and widely used.

The distribution of residual thermal stress in EBAM and SLM processes has been studied by many researchers, such as Denlinger et al. [23], Cao et al. [24] and Liu et al. [25]. Many of these methods are complicated, expensive or time consuming, and they cannot measure residual stress at microstructure scale interested. Comparatively, the residual stress measurement by Vickers micro-indentation [17, 26] is possibly an appropriate method for the rapid evaluation of residual stress in microstructure scale. Cao et al. [24] has studied the effect of overlap rate on the residual stress in as-deposited LSF Inconel 718 samples, and he found that the overlap area possesses higher residual stress compared with the inner-pass area, and the position of peak residual stress is closer to previous pass. Besides, increasing of the overlap rate will broaden the variation range of the residual stress. According to the results of Liu et al. [25], there is an alternative distribution between high residual stress regions and low residual stress regions within a single deposited layer. In the present study, the residual stress in as-deposited Ti-6Al-4V and Inconel 718 samples prepared by EBAM and SLM, separately, have been investigated. The microstructure of them also have been analyzed.

## **2. Methodology**

According to the studies of Carlsson and Larsson [18, 19], the residual strain fields can be accurately correlated with the hardness value, and residual stresses can be related to the size of the

contact area. In the Vickers test, even though it is assumed that elastic recovery does not occur once the load is removed, elastic recovery does occur and sometimes its influence is quite remarkable. As shown in the Figure 1, the impression shape is distorted due to elastic recovery, which is very common in anisotropic materials.

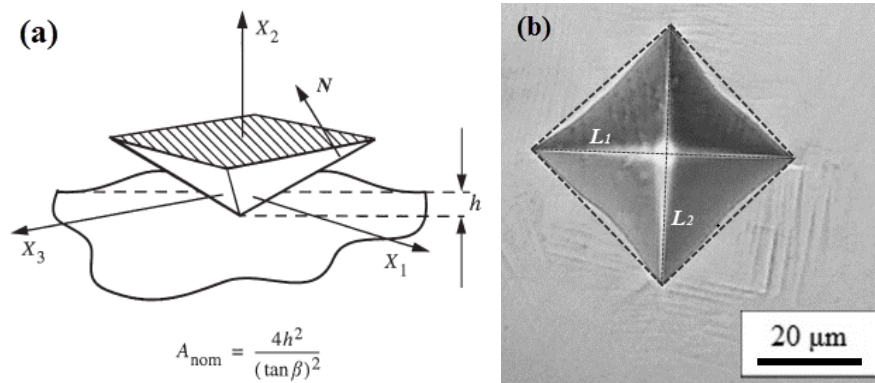


Figure 1. (a) Schematic of the geometry of the Vickers indentation tests, and (b) Schematic of the nominal projected contact area  $A_{nom}$

In order to establish a correlation between the equibiaxial residual stress/strain fields and the contact area/indentation hardness, a new indentation parameter ( $c^2$ ) was introduced in their model to calculate the residual stress for a sharp indentation,

$$c^2 = \frac{A_{real}}{A_{nom}} \quad (1)$$

where  $A_{real}$  represents the real contact area of a sample showing sink-in or pile-up, and  $A_{nom}$  is the nominal contact area directly calculated from the indentation depth ( $h_{max}$ ) without consideration of sink-in or pile up along the contact boundary,

$$A_{nom} = \left( \frac{2h_{max}}{\tan 22^\circ} \right)^2 = 24.5h_{max}^2 \quad (2)$$

Carlsson et al.'s model can be expressed as the following form,

$$c^2 = c_0^2 - 0.32 \ln \left( 1 + \frac{\sigma_{res}}{\sigma(\epsilon_{res})} \right) \quad (3)$$

where  $\epsilon_{res}$  is the residual plastic strain that can be deduced from the changes of hardness according to Tabor's equation [7],  $\sigma(\epsilon_{res})$  is the flow stress when the effective plastic strain equals to  $\epsilon_{res}$ .  $c^2$  and  $c_0^2$  are the area ratios for the case with both residual stresses and residual strains and original material, respectively. The detail of the methodology can be seen in the former study [27].

### 3. Experiments

With Arcam S12 EBAM machine and Concept Laser M2 SLM machine, the Ti-6Al-4V parts and Inconel 718 parts used in this study were manufactured, respectively, at NASA's Marshall Space Flight Center (Huntsville, AL). The Ti-6Al-4V parts were built with the pre-alloyed Ti-6Al-4V powders as the raw material, the chemical compositions of which are 6.0% Al, 4.0% V, 0.03% C, 0.1% Fe, 0.15% O, 0.01% N, 0.003% H and the remains is Ti. The major diameter of the powder is around 30 to 50  $\mu\text{m}$  [28]. With CAD software, the model of the parts with dimension of 60 mm  $\times$  5.5 mm  $\times$  25mm (L  $\times$  W  $\times$  H) was built and imported into the machine. The detail of the manufacturing can be found in the previous studies [25, 29, 30]. In this study, the

Ti-6AL-4V parts were built with four different beam scanning speeds, which is achieved by control the speed function (SF=20, 36, 50 and 65) in the Arcam EBAM systems.

The Inconel 718 part, which is a block with length of 40 mm, width of 40 mm and height of 6 mm, were first modeled by CAD software and then fabricated layer by layer. The weight percent of elements in the fine pre-alloyed Inconel 718 powder are 54.7% Ni, 18.3% Cr, 18.9% Fe, 4.6% Nb, 2.0% Mo, and 0.83% Ti. The detail of the manufacturing process can be seen in former studies .

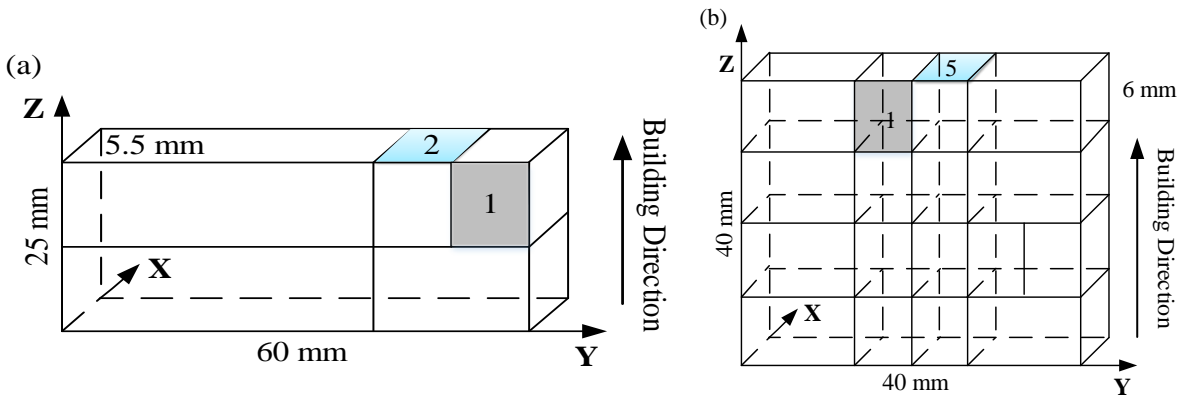


Figure 2. Samples location on the parts: (a) Ti-6Al-4V, and (b) Inconel 718

The specimens used for Vickers indentation test and microstructural analysis were cut directly from the as-deposited parts, respectively, by electrical discharge machining (EDM), the position of them in the parts are illustrated in Figure 2. The size of the specimens for the Ti-6Al-4V and Inconel 718 are  $12 \times 11 \times 5.5$  and  $6 \times 10 \times 6$  cm, respectively. Specimens of different cross-sections (scanning surface: Z-plane, build side surface: X-plane) were prepared to examine the anisotropic conditions in microstructures. Then, they were processed with standard metallographic procedures, such as mounting, grinding with SiC papers up to the grit size of 1200. In order to decrease the effect of the EDM cutting on the residual stress, all the test surfaces of specimen are grinded to the central surface of them. After that, they were polished with diamond suspension down to  $0.5 \mu\text{m}$ . After finishing polishing, the specimens were cleaned by ultrasonic oscillator with distilled water about 1 minute to reduce the influence of surface work hardening.

The microindentation test were run on each surface of specimens with a pattern of 3 by 3 matrix, and each element has run 4 by 4 tests. To reveal the microstructures, polished specimens were then etched with an acid-based solution: 20 ml hydrochloric acid (37 wt. %) and 20 ml (60 wt. %) nitric acid, and 1 g copper chloride [29]. The etched metallographic samples were examined using a Leitz optical microscope (OM) and a JEOL 7000 scanning electron microscope (SEM).

### **3. Results and discussion**

#### **3.1 Microstructure analysis**

The microstructure of Ti-6Al-4V on the X-plane (Side Surface) are shown in Figure 3-(b). Typically, Ti-6Al-4V samples from EBAM show an ordered lamellar microstructure, consisting of extremely fine grains due to small melt pool and rapid cooling in the EBAM process. It can be seen that the bulk microstructure in the side surface of the solid part is made up of columnar prior

$\beta$  grains delineated by grain boundary  $\alpha$  and growing along the build direction. The width of the columnar structure ranges from 25 to 50  $\mu\text{m}$  in the current study.

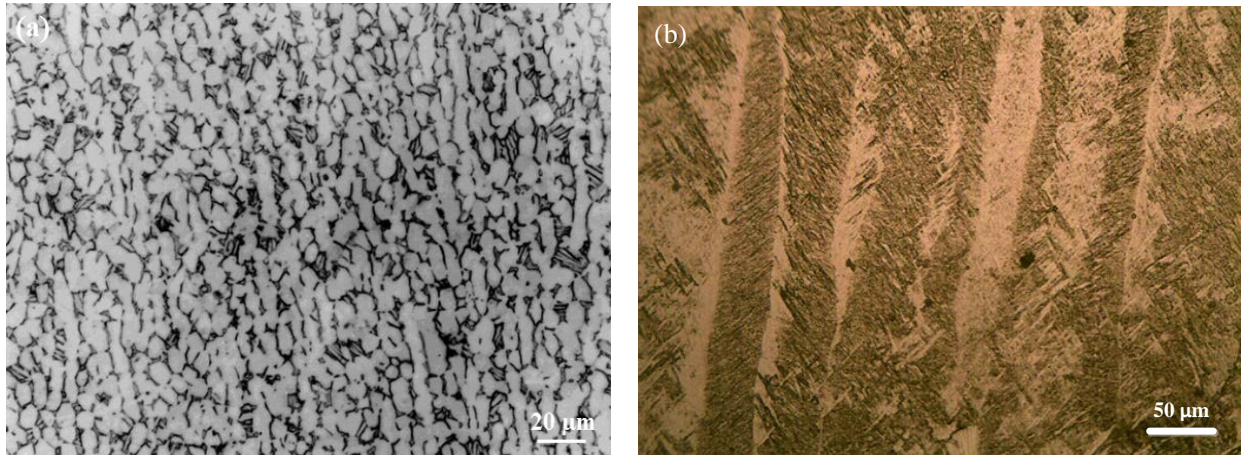


Figure 3. Microstructures of Ti-6Al-4V samples: (a) Casting [31] and (b) EBAM

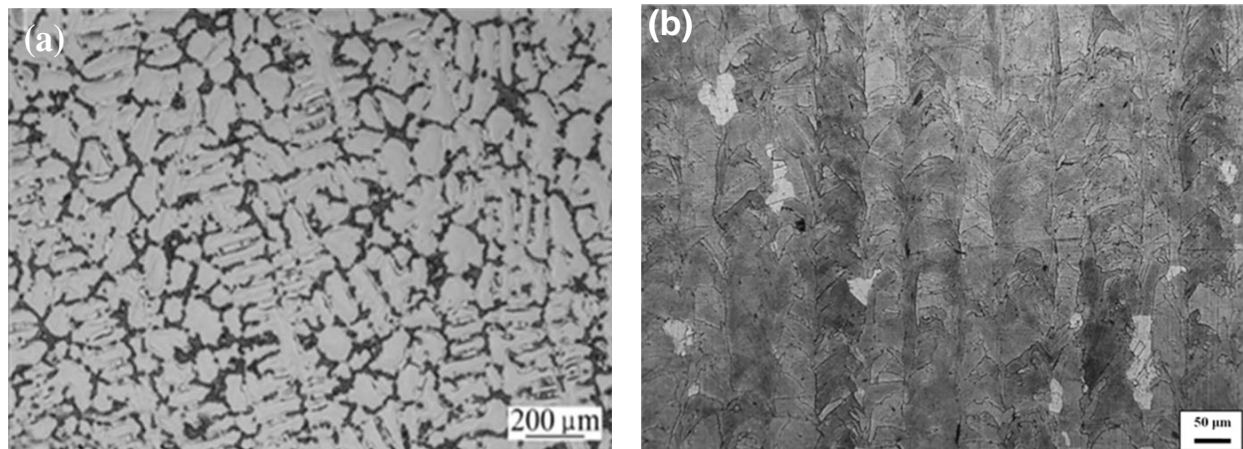


Figure 4. Microstructures of Inconel 718 samples: (a) Casting [7] and (b) SLM

For the cast specimen, as shown in Figure 3-(a), a typical  $\alpha$ -case microstructure consisting of columnar  $\alpha$ -crystals can be clearly observed, which is not as fine & ordered as that in EBAM specimens. Same case has been observed in Inconel 718. Take casting, one of the traditional manufacturing methods, as an example, the components present coarse grain size, heavy dendritic segregation, which is caused by the low cooling rate during solidification, as shown in Figure 4 (a) [7]. Besides, solidification defects, such as shrinkage cavities and porosity, also form in the castings at the same time. Thus, homogenization treatment and hot isostatic pressing (HIPing) are required to homogenize the microstructure, to close the internal pores and to improve the casting quality [32]. However, with the new AM technologies, such as SLM, the specimen shows fine microstructure due to rapid cooling rate. Figure 4 (b) demonstrates the detailed microstructures of the as-deposited Inconel 718 sample. It can be seen that fine dendrites are formed within the column grain.

From the microstructure in the Z-plane (scanning surface), as shown in Figure 5, the grain size of the “equiaxed” type grains which represents the head of the columnar grains formed in the

side surface. The grain size of equiaxed structure is comparable to the width of the columnar grains. Such equiaxed grains in the scanning surface are also found by other researchers [33]. It could demonstrate that the columnar structure is generally rod-shaped. Besides, for the Inconel 718, the repeating unit of the pattern could also be seen in the Z-plane, which is based on a square with the length of the side around 100  $\mu\text{m}$ .

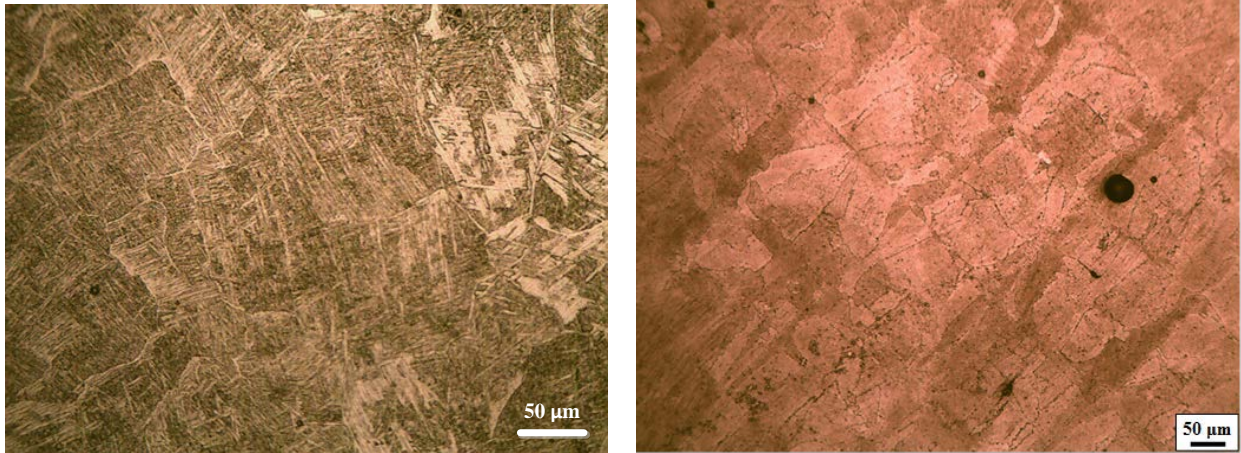


Figure 5. Microstructures on X-Plane of samples: (a) Ti-6Al-4V (L) and (b) Inconel 718 (R)

### 3.2 Residual Stresses

Generally, the residual stress is unevenly distributed in the parts based on the results calculated. For the as deposited Ti-6AL-4V specimens, some test points almost have none residual stress, while some other test points have very big compressive stress and the maximum absolute value is around 180 MPa, which is about 20 percent of the yield strength ( $\sim 860$  MPa) of Ti-6Al-4V. The average value of the residual stresses in the Z-plane and X-plane both are compressive stress, as shown in Figure 6. As to the Inconel 718 samples, some test points have an maximum absolute value around 350 MPa, which is about 30 percent of the yield strength of Inconel 718 ( $\sim 900$  MPa [34]). The average value of the residual stresses in the Z-plane and X-plane samples are compressive and tensile stress, respectively, as shown in Figure 7.

It is known to all that the all the parts were built layer by layer, which means the latter melting layer will re-melt or reheat the former layers. During this process, the latter layer will give the former layers a compressive residual stress, which can be seen from the Figure 6(a) and Figure 7(a). The exception is the residual stress in the Z-plan of the Inconel 718 parts, which is contributed to the special designed scanning pattern. During the manufacturing process, the deposited powder layer will be melted selectively according to the predefined scanning path with the pattern of repeating unit of a 100  $\mu\text{m}$  square, as can be seen in Figure 5 (b), which will minimize the residual stress in the part. In this way, the latter solid patterns will have a tensile stress on the former melt solid patterns on the same layer and the former layer will also have a tensile stress on this latter melt layer, which will excess the compressive stress exerted by the following melting layer. Therefore, the residual stress in the Z-plane will be tensile stress in general.

Besides, it is also can be seen that there is no significant changing trend along the building direction of the Inconel 718 parts. Even through there is a little bit increasing trend for the average

value in the Z-plane, it has a pretty high standard deviation, which also has been mentioned by Liu et al. [25] and Cao et al.[24]. It was caused by the inhomogeneity of properties in the microstructure as the parts produced. In the study of Sebastiani et al.[35], the author said that the big standard deviation of the calculated residual stress (0.85 GPa) is likely to be caused by the real variation of residual stress from point to point, probably due to the nonhomogeneity of the WC–Co substrate. There are also some error introduced by the manual measurement in measuring the area and length of the diagonal lines.

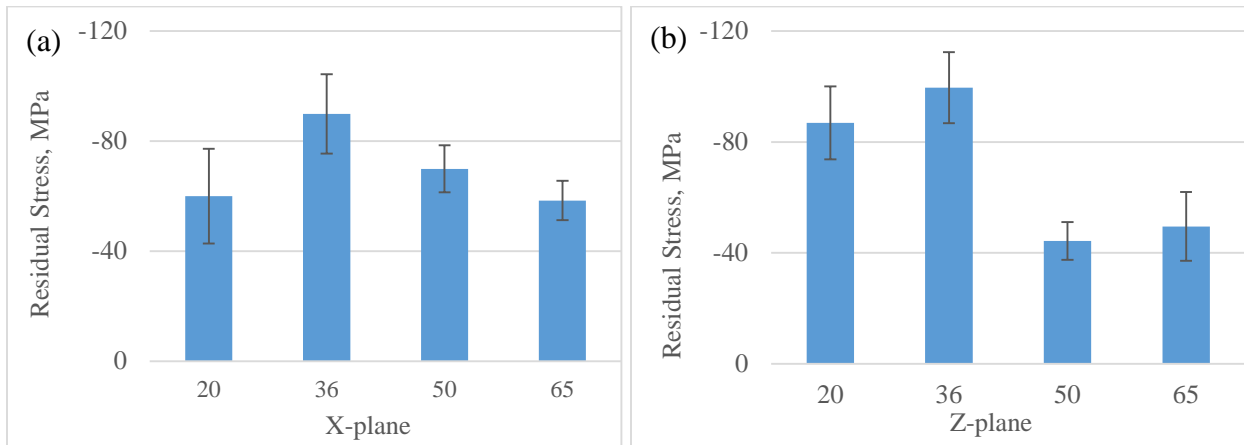


Figure 6. Residual stress in the Ti-6Al-4V parts (EBAM process)

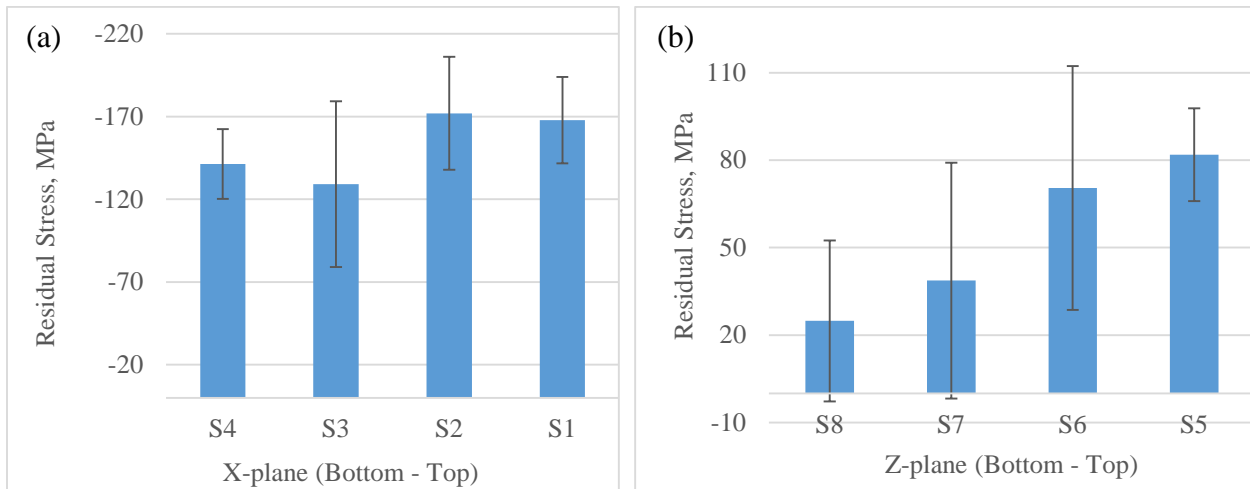


Figure 7. Residual stress in the Inconel 718 samples (SLM process)

There is another thing need to mention that the EBAM process produced parts have smaller residual stress than the parts made with SLM process, which can be seen by comparing of the Figure 6 and Figure 7. One of the reasons is the EBM process takes place in vacuum at high temperature. Thus, the EBM process has a slower cools down rate than that in SLM process, which will result in stress relieved components. The other one is the electron beam will preheat the base plate or the entire powder to an optimal ambient temperature before the melting process of the powder in the build. As a result, the parts produced with the EBAM process have less stress than the laser-beam produced samples.

### 3.3 Microhardness

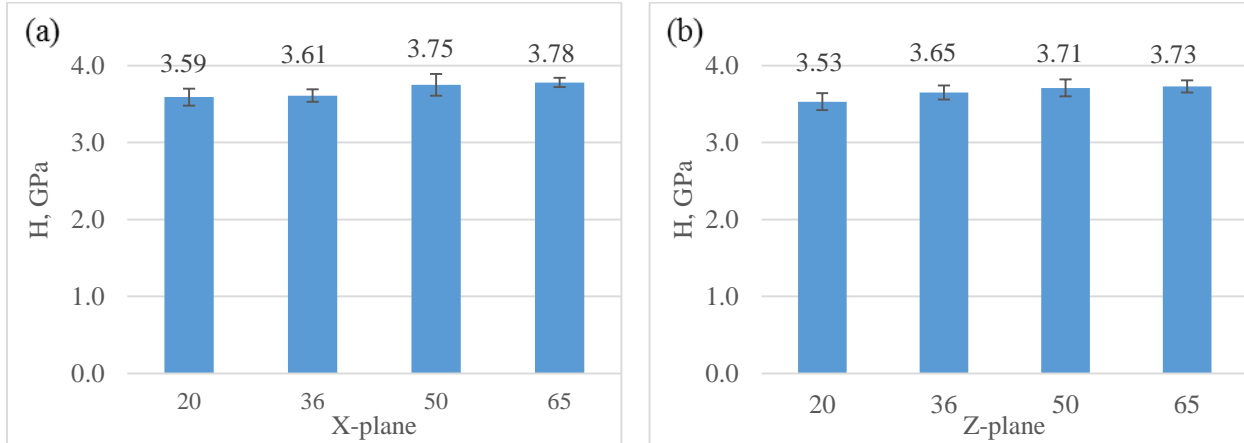


Figure 8. Hardness of Ti-6Al-4V specimens built with different SFs

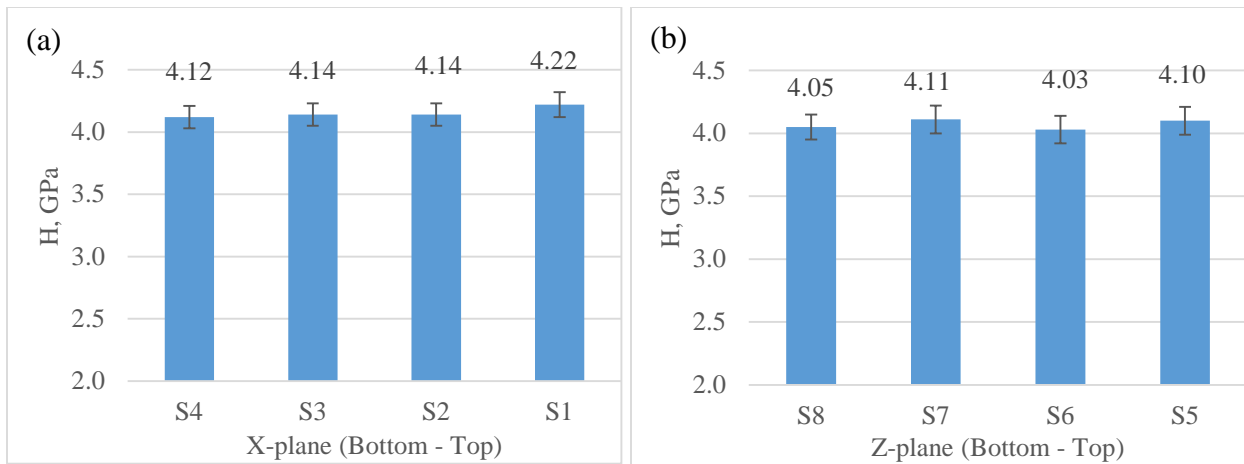


Figure 9. Vickers' hardness on the surface of the Inconel 718 samples

The microhardness values of as-deposited Ti-6Al-4V and Inconel 718 are shown in Figure 8 and Figure 9, respectively. It can be seen that the residual stress almost do not have influence on the micro-hardness of the parts. For the Ti-6Al-4V parts, the microhardness will increase with the increasing of electron beam scanning speed, but this changing trend is not very significantly if incorporating the standard deviation of the hardness. Generally, this test results are accord with our former results [36]. Besides, the EBAM samples also show higher micro-hardness than that of the cast or wrought specimens, which has also been mentioned by Koike et al. [37]. He said it is probably attributed to finer  $\alpha/\beta$  lamellar microstructures. they are comparable/superior to the cast/wrought parts.

For the Inconel 718 parts, the Vickers hardness are comparable to the parts build with other technologies. According to Amato et al. [38], the micro-indentation (Vickers) hardness was 3.9 GPa for the as-fabricated materials, 5.7 GPa for the HIP material, and 4.6 GPa for the annealed material. This also has been reported by Zhao et al. [39], the average hardness for heat treated samples is HRC 41, which has increased remarkably from HRC17 for as-deposited samples. Thus,

the Vickers hardness of the parts built with the SLM process is comparable to other manufacturing methods.

#### **4. Conclusion**

With Vickers micro-indentation method, the residual stress in the Ti-6Al-4V parts and Inconel 718 parts manufactured by EBAM (Electron Beam Additive Manufacturing) and SLM (Selective Laser Melting), respectively, have been investigated with the methodology established by Carlsson et al., a mechanical instrumented indentation technique, which is based on the experimental correlation between the indentation characteristic and the residual stress.

The results show that the residual stress is unevenly distributed in the parts. For the Ti-6Al-4V parts, the average residual stress in both Z-plane and X-plane are compressive stress, while the Inconel 718 SLM parts show a tensile stress and a compressive stress in the Z-plane and X-plane, respectively. By comparing the residual stress results, the Ti-6Al-4V parts have lower absolute value of residual stress than the Inconel 718 parts. However, the residual stress almost do not have influence on the micro-hardness of the Ti-6Al-4V and Inconel 718 parts. Moreover, the Vickers hardness values of the parts built using SLM and EBAM are comparable to the literature data. Besides, the microstructure of the parts also has been studied and compared to that obtained with traditional methods.

#### **Acknowledgements**

The author gratefully thanks NASA and CFDRG for their support and also thanks Dr. Xibing Gong for the microstructure analysis work in this study.

#### **References:**

- [1] Wu, X., Liang, J., Mei, J., Mitchell, C., Goodwin, P. S., and Voice, W., 2004, "Microstructures of laser-deposited Ti-6Al-4V," *Materials & Design*, 25(2), pp. 137-144.
- [2] Gong, X., Lydon, J., Cooper, K., and Chou, K., 2014, "Beam speed effects on Ti-6Al-4V microstructures in electron beam additive manufacturing," *Journal of Materials Research*, 29(17), pp. 1951-1959.
- [3] Vilaro, T., Colin, C., and Bartout, J.-D., 2011, "As-fabricated and heat-treated microstructures of the Ti-6Al-4V alloy processed by selective laser melting," *Metall and Mat Trans A*, 42(10), pp. 3190-3199.
- [4] Dadbakhsh, S., and Hao, L., 2012, "Effect of Al alloys on selective laser melting behaviour and microstructure of in situ formed particle reinforced composites," *Journal of Alloys and Compounds*, 541(0), pp. 328-334.
- [5] Dong, L. X., and Wang, H. M., 2008, "Microstructure and corrosion properties of laser-melted deposited Ti<sub>2</sub>Ni<sub>3</sub>Si/NiTi intermetallic alloy," *Journal of Alloys and Compounds*, 465(1-2), pp. 83-89.
- [6] Zhang, B., Liao, H., and Coddet, C., 2013, "Selective laser melting commercially pure Ti under vacuum," *Vacuum*, 95(0), pp. 25-29.
- [7] Yadroitsev, I., and Smurov, I., 2010, "Selective laser melting technology: From the single laser melted track stability to 3D parts of complex shape," *Physics Procedia*, 5, Part B(0), pp. 551-560.

- [8] Wang, X., Gong, X., and Chou, K., "Review on powder-bed laser additive manufacturing of Inconel 718 parts," Proc. ASME 2015 International Manufacturing Science and Engineering Conference, American Society of Mechanical Engineers, p. V001T001A002.
- [9] Withers, P., and Bhadeshia, H., 2001, "Residual stress. Part 1—measurement techniques," *Materials science and Technology*, 17(4), pp. 355-365.
- [10] Liu, W., Kong, F., and Kovacevic, R., "Residual Stress Analysis and Weld Bead Shape Study in laser welding of high strength steel," Proc. ASME 2013 International Manufacturing Science and Engineering Conference collocated with the 41st North American Manufacturing Research Conference, American Society of Mechanical Engineers, pp. V001T001A053-V001T001A053.
- [11] Liu, W., Ma, J., Kong, F., Liu, S., and Kovacevic, R., 2015, "Numerical Modeling and Experimental Verification of Residual Stress in Autogenous Laser Welding of High-Strength Steel," *Lasers in Manufacturing and Materials Processing*, 2(1), pp. 24-42.
- [12] Qian, Z., Chumbley, S., Karakulak, T., and Johnson, E., 2013, "The residual stress relaxation behavior of weldments during cyclic loading," *Metall and Mat Trans A*, 44(7), pp. 3147-3156.
- [13] Qian, Z., Chumbley, S., and Johnson, E., 2011, "The effect of specimen dimension on residual stress relaxation of carburized and quenched steels," *Materials Science and Engineering: A*, 529, pp. 246-252.
- [14] Fischer, W., Malzbender, J., Blass, G., and Steinbrech, R. W., 2005, "Residual stresses in planar solid oxide fuel cells," *Journal of Power Sources*, 150(0), pp. 73-77.
- [15] Gouldstone, A., Chollacoop, N., Dao, M., Li, J., Minor, A. M., and Shen, Y.-L., 2007, "Indentation across size scales and disciplines: Recent developments in experimentation and modeling," *Acta Materialia*, 55(12), pp. 4015-4039.
- [16] Tsui, T., Oliver, W., and Pharr, G., 1996, "Influences of stress on the measurement of mechanical properties using nanoindentation: Part I. Experimental studies in an aluminum alloy," *Journal of Materials Research*, 11(03), pp. 752-759.
- [17] Suresh, S., and Giannakopoulos, A. E., 1998, "A new method for estimating residual stresses by instrumented sharp indentation," *Acta Materialia*, 46(16), pp. 5755-5767.
- [18] Carlsson, S., and Larsson, P. L., 2001, "On the determination of residual stress and strain fields by sharp indentation testing.: Part I: theoretical and numerical analysis," *Acta Materialia*, 49(12), pp. 2179-2191.
- [19] Carlsson, S., and Larsson, P. L., 2001, "On the determination of residual stress and strain fields by sharp indentation testing.: Part II: experimental investigation," *Acta Materialia*, 49(12), pp. 2193-2203.
- [20] Chen, G., Singh, D., Eryilmaz, O., Routbort, J., Larson, B. C., and Liu, W., 2006, "Depth-resolved residual strain in MoN/Mo nanocrystalline films," *Applied physics letters*, 89(17), p. 172104.
- [21] Lee, Y.-H., and Kwon, D., 2003, "Measurement of residual-stress effect by nanoindentation on elastically strained (100) W," *Scripta Materialia*, 49(5), pp. 459-465.
- [22] Wang, Q., Ozaki, K., Ishikawa, H., Nakano, S., and Ogiso, H., 2006, "Indentation method to measure the residual stress induced by ion implantation," *Nuclear Instruments and Methods in Physics Research Section B: Beam Interactions with Materials and Atoms*, 242(1-2), pp. 88-92.
- [23] Denlinger, E. R., Heigel, J. C., and Michaleris, P., 2014, "Residual stress and distortion modeling of electron beam direct manufacturing Ti-6Al-4V," *Proceedings of the Institution of Mechanical Engineers, Part B: Journal of Engineering Manufacture*, p. 0954405414539494.

- [24] Cao, J., Liu, F., Lin, X., Huang, C., Chen, J., and Huang, W., 2013, "Effect of overlap rate on recrystallization behaviors of Laser Solid Formed Inconel 718 superalloy," *Optics & Laser Technology*, 45(0), pp. 228-235.
- [25] Liu, F., Lin, X., Yang, G., Song, M., Chen, J., and Huang, W., 2011, "Microstructure and residual stress of laser rapid formed Inconel 718 nickel-base superalloy," *Optics & Laser Technology*, 43(1), pp. 208-213.
- [26] Chen, C., Pan, C., and Fu, Q., 2007, "Micro-residual stress measurement using Vickers micro-indentation," *Mater Mech Eng*, 1, pp. 8-11.
- [27] Wang, X., and Chou, K., "A Method to Estimate Residual Stress in Metal Parts Made by Selective Laser Melting," *Proc. ASME 2015 International Mechanical Engineering Congress and Exposition*, American Society of Mechanical Engineers, p. V02AT02A002.
- [28] Chlebus, E., Kuźnicka, B., Kurzynowski, T., and Dybała, B., 2011, "Microstructure and mechanical behaviour of Ti—6Al—7Nb alloy produced by selective laser melting," *Materials Characterization*, 62(5), pp. 488-495.
- [29] Li, L., Guo, Y., Wei, X., and Li, W., 2013, "Surface integrity characteristics in wire-EDM of Inconel 718 at different discharge energy," *Procedia CirP*, 6, pp. 220-225.
- [30] Gong, X., Anderson, T., and Chou, K., "Review on powder-based electron beam additive manufacturing technology," *Proc. ASME/ISCIE 2012 International Symposium on Flexible Automation*, American Society of Mechanical Engineers, pp. 507-515.
- [31] Murr, L. E., Esquivel, E. V., Quinones, S. A., Gaytan, S. M., Lopez, M. I., Martinez, E. Y., Medina, F., Hernandez, D. H., Martinez, E., Martinez, J. L., Stafford, S. W., Brown, D. K., Hoppe, T., Meyers, W., Lindhe, U., and Wicker, R. B., 2009, "Microstructures and mechanical properties of electron beam-rapid manufactured Ti-6Al-4V biomedical prototypes compared to wrought Ti-6Al-4V," *Materials Characterization*, 60(2), pp. 96-105.
- [32] Kruth, J.-P., Mercelis, P., Van Vaerenbergh, J., Froyen, L., and Rombouts, M., 2005, "Binding mechanisms in selective laser sintering and selective laser melting," *Rapid prototyping journal*, 11(1), pp. 26-36.
- [33] Al-Bermani, S., Blackmore, M., Zhang, W., and Todd, I., 2010, "The origin of microstructural diversity, texture, and mechanical properties in electron beam melted Ti-6Al-4V," *Metall and Mat Trans A*, 41(13), pp. 3422-3434.
- [34] Wang, Z., Guan, K., Gao, M., Li, X., Chen, X., and Zeng, X., 2012, "The microstructure and mechanical properties of deposited-IN718 by selective laser melting," *Journal of Alloys and Compounds*, 513(0), pp. 518-523.
- [35] Sebastiani, M., Bemporad, E., Schwarzer, N., and Carassiti, F., 2014, "Effects of Residual Stress on Nano-Mechanical Behavior of Thin Films," *Nanomechanical Analysis of High Performance Materials*, A. Tiwari, ed., Springer Netherlands, pp. 263-284.
- [36] Wang, X., Gong, X., and Chou, K., 2015, "Scanning Speed Effect on Mechanical Properties of Ti-6Al-4V Alloy Processed by Electron Beam Additive Manufacturing," *43rd Proceedings of the North American Manufacturing Research* Charlotte, NC, pp. 1-9.
- [37] Gockel, J., and Beuth, J., 2013, "Understanding Ti-6Al-4V microstructure control in additive manufacturing via process maps," *Solid Freeform Fabrication Proceedings*, Austin, TX, Aug, pp. 12-14.
- [38] Amato, K., Gaytan, S., Murr, L., Martinez, E., Shindo, P., Hernandez, J., Collins, S., and Medina, F., 2012, "Microstructures and mechanical behavior of Inconel 718 fabricated by selective laser melting," *Acta Materialia*, 60(5), pp. 2229-2239.

[39] Zhao, X., Chen, J., Lin, X., and Huang, W., 2008, "Study on microstructure and mechanical properties of laser rapid forming Inconel 718," *Materials Science and Engineering: A*, 478(1-2), pp. 119-124.